Contrib Mineral Petrol (2000) 139: 273–284

B. Cesare

Incongruent melting of biotite to spinel in a quartz-free restite at El Joyazo (SE Spain): Textures and reaction characterization

Received: 1 June 1999 / Accepted: 8 February 2000

Abstract In the Grt-Bt-Sil restitic xenoliths of El Joyazo (Cerro de Hoyazo), hercynitic spinel is a minor phase commonly associated with biotite. The possible reaction relationships among biotite and spinel are studied in reaction textures developed around biotites at their contact with patches of fibrolitic sillimanite and rhyolitic melt. In these textures, resorbed biotite crystals about 1 mm long are rimmed by a layer of glass <200 μm thick containing spinel and ilmenite; the same glass also fills embayments in biotite. Spinel forms euhedral crystals <100 μm in size, and ilmenite occurs as smaller anhedral crystals or needles, often intergrown with spinel. The homogeneous felt-like melt-sillimanite aggregate (“mix”) is richest in glass close to the reaction rim around biotite. Plagioclase and garnet are located >5 mm away from the reaction texture. Biotite is chemically zoned. Cores (Bt_1) have $X_{Mg} = 0.35 \pm 0.02$ and $Ti = 0.58 \pm 0.01$ atoms; whereas the outer rims (Bt_2) have $X_{Mg} = 0.45 \pm 0.01$ and Ti up to 0.68 atoms. The hercynite-rich spinel (*Spl*) has low ZnO content (<0.80 wt%) and $X_{Mg} = 0.26 \pm 0.04$. The chemical compositions of the *mix* aggregate represent linear combinations between sillimanite and a silica-rich melt. This melt ($melt_1$) is different from that of the layer around biotite ($melt_2$), which is also richer in Ca and alkalis. Garnet rims (*Grt*) have low Ca and Mn, and $X_{Mg} = 0.14$. Plagioclase is characterized by large homogeneous cores (Pl_1, $An_{31 \pm 2}$) and more calcic rims (Pl_2, $An_{49 \pm 6}$). Matrix analysis in the 9-component (Al-Ca-Fe-K-Mg-Mn-Na-Si-Ti), 9-phase (Bt_1-Bt_2-Grt-Spl-Ilm-$melt_2$-mix-Pl_1-Pl_2) system provides the mass balance (in mole units):

$$0.78Bt_1 + 1.95Pl_1 + 2.82mix + 0.32Grt = 0.25Ilm + 5.00melt_2 + 0.30Bt_2 + 2.53Spl + 1.03Pl_2$$

This relationship is in excellent agreement with the observed textures and hence is considered a good model for the incongruent melting of biotite in the xenoliths. The mass-balance indicates that melt production is dominated by the availability of K from biotite, and that garnet and plagioclase must be involved as reactants, so that the reaction volume is larger than the melt production site. The melting of biotite, constrained at $T = 900$–950°C and $P \geq 5$ kbar, is not a terminal reaction, as its variance in the reduced 8-component multisystem is ≥3.

Supplementary material. Table e1. Electron microprobe (EMP) analyses of biotites from sample HO42, based on 24 oxygens and 4 OH, Table e2. EMP analyses of $melt_2$ glasses from sample HO42, based on 5 oxygens, and CIPW norm, Table e3. EMP analyses of ilmenite from sample HO42, based on 2 cations and 3 oxygens, Table e4. EMP analyses of plagioclase from sample HO42, based on 8 oxygens, Table e5. EMP analyses of mix from sample HO42, based on 5 oxygens, Table e6. EMP analyses of spinels from sample HO42, based on 3 cations and 4 oxygens, have been deposited in electronic form and can be obtained from http://link.springer.de/link.service/journals/00410

B. Cesare (✉)
Dipartimento di Mineralogia e Petrologia,
Università di Padova, Corso Garibaldi 37, 35137 Padova, Italy
e-mail: bernardo@dmp.unipd.it

Editorial responsibility: J. Hoefs

Introduction

The incongruent melting of biotite is considered the most important cause of simultaneous generation of granitic melts and granulite-facies restitic rocks at low to intermediate pressures (e.g. Thompson 1982; Vielzeuf and Holloway 1988), therefore, the characterization of this reaction is crucial to the understanding of several related phenomena taking place during high grade metamorphism and crustal anatexis.

In the study of natural granulites and migmatites, an uncertainty in the modelling of biotite melting reactions is that compositions of minerals now in the rocks may be affected by modification on cooling; this is frequently observed by incompatibility of geothermobarometric estimates with phase assemblage indications (e.g. Fitzsimons and Harley 1994), or by back reaction between

restite and melt (Kriegsman and Hensen 1998). The second major drawback is that the melt produced can rarely be recognised and analysed, either because it has been extracted from the observable residue, or because it has been modified by re-equilibration. Both problems have been clearly pointed out by Grant (1985) who noted that what is discussed as partial melting in pelitic migmatites is often attributable to re-crystallization.

Apart from rare studies of natural examples (e.g. Grapes 1986; Brearley 1987), partial melting of biotite-bearing rocks has been extensively investigated by experimental modelling, which has concentrated on the behaviour of pelitic compositions and on greywackes, the latter being considered the more fertile sources. Most of the experimental work (summarized by Carrington and Harley 1995) has been performed in KFMASH Qtz-saturated systems (mineral abbreviations after Kretz 1983; Gph = graphite), aimed at defining the *P-T* conditions, the melt productivities, and the restite assemblages of the various Bt-melting equilibria at various degrees of H_2O saturation. Recently, increasing attention has been paid to more complex systems, accounting for the presence of Na, Ca, and Ti in natural rocks. As concerns Ti, it has been demonstrated that its presence has a dramatic stabilizing effect on biotite (see Stevens et al. 1997 for a listing of previous studies).

Depending on *P–T* conditions and bulk composition (e.g. the degree of saturation in alumina or silica), the granulite facies residue of biotite incongruent melting is characterized by one or more of the ferromagnesian phases cordierite, garnet, orthopyroxene and Fe-Mg-Al spinel. The latter is a typical product of biotite melting in Qtz-undersaturated systems (Harris 1981; Grant 1985). Unless it is stabilized to lower *T* by the presence of Zn, the coexistence of spinel + quartz requires temperatures in excess of 800 °C (Vielzeuf 1983; Montel et al. 1986).

The relationships among biotite and hercynitic spinel in Qtz-undersaturated, Sil-bearing assemblages have been outlined by Montel et al. (1986), who described and interpreted natural occurrences, discussed the stabilizing effect of Zn, and proposed a schematic petrogenetic grid in the KFASH(Zn) system. They concluded that Zn-poor spinels formed by melting of biotite-sillimanite assemblages are an indication for advanced Qtz-depleted conditions of anatexis; they also noted that garnet (or cordierite at lower pressure) should be a reactant in the melting reactions. There have been few additional experimental or theoretical studies on this subject, so that modelling of natural biotite-spinel melting reactions in granulites is far from adequately and quantitatively constrained.

This work aims to help fill this gap, by studying a natural example of biotite melting in the xenoliths of El Joyazo (also called Cerro de Hoyazo, SE Spain). The peculiar geological setting of these rocks, representing restites of mid-crustal provenance enclosed in dacitic lavas, allows detailed characterization of both textural and chemical features of the melting reaction, and monitoring of systematic chemical variations in minerals and melt. These results are compared with data from relevant experimental studies, and used for evaluating reaction stoichiometry by a model mass balance in the KFMASH-Ti-Ca-Na-Mn system.

Geological background and petrography

The Neogene dacitic dome of El Joyazo contains abundant aluminous xenoliths (Zeck 1968, 1970), the most representative of which are characterized by the assemblage Grt-Bt-Sil-Pl-Gph-Ap-melt (Fig. 1). Cesare et al. (1997) interpreted these rocks, hereinafter referred to as (Grt-Bt-Sil) *xenoliths*, as the residue after extraction of 30–60 wt% of rhyolitic melt from metapelitic protoliths similar to those exposed in the adjacent Betic Cordillera; they observed that the melt is preserved in the xenoliths as both intergranular glass films and glass inclusions within all mineral phases. This melt ($melt_1$) formed during the first, main event of partial melting that occurred under fluid-present conditions (Cesare and Maineri 1999) at about 5–7 kbar and 850 ± 50 °C, as a result of the thermal anomaly that accompanied lithospheric thinning and upwelling of the upper mantle during the opening of the Alboran Sea (De Larouziere et al. 1988; Platt et al. 1996; Zeck 1996).

The xenoliths have been described in detail by Zeck (1970) and Cesare et al. (1997); they are virtually Qtz-free (quartz is only observed as inclusions in garnet or plagioclase) and biotite constitutes up to 40% of the rocks. The persistence of biotite at temperatures of about 850 °C can be explained by the absence of quartz and the stabilizing effect of titanium. For the purpose of this study, the behaviour of the additional phases ilmenite, hercynite, K-feldspar, and cordierite needs careful consideration. Cordierite is present in about one third of the xenoliths; it forms large, spongy poikiloblasts up to 10 cm in size, generally devoid of melt inclusions. In most cases the cordierite post-dates the development of the main assemblage Grt-Bt-Sil-Pl-melt. Textural relationships between garnet and cordierite do not indicate replacement due to decompression, an observation supported by the similar results of barometric estimates in Crd-bearing and Crd-free Grt-Bt-Sil xenoliths (Cesare et al. 1997).

Ilmenite occurs sporadically, and mostly in Spl-bearing xenoliths. Large, anhedral ilmenite grains in Spl-free xenoliths are probably remnants of the metasedimentary protolith, as they do not contain melt inclusions. K-feldspar is generally absent in the xenoliths, and is only present as rare rims around plagioclase in contact with interstitial melt.

Green or brown-green hercynitic spinel (*spinel*) is observed as an accessory phase (< 1 %vol) in about half of the xenoliths; it

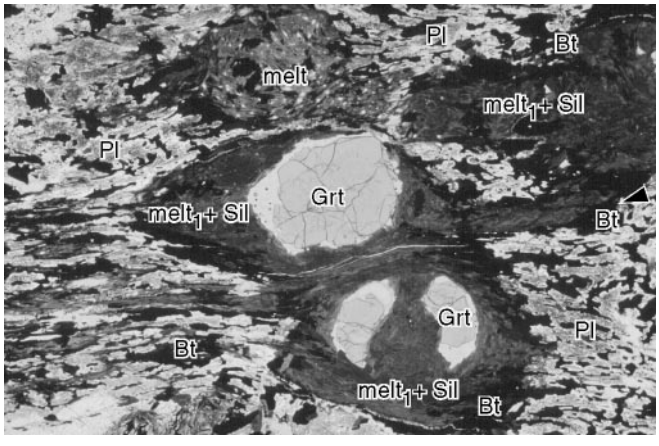

Fig. 1 Photomicrograph showing the general appearance of the Grt-Bt-Sil xenoliths of El Joyazo. Plane-polarized light, width of view 22 mm

forms euhedral crystals < 2 mm, often associated with biotite or garnet and/or glass. In some xenoliths spinel is more abundant (2–3 %vol); one of these xenoliths (HO42) is the sample in which the spinel-biotite relationships have been most extensively studied, and is described in detail in the next section. The gahnite content of spinel is generally very low (see also Table 2 in Cesare et al. 1997), which indicates that, in this case, phase equilibria involving spinel are not affected by the extra-component Zn.

Textures of biotite melting

Sample HO42 is a typical xenolith from El Joyazo: it has a rounded shape and is about 10 cm in diameter; it has a medium grain-size with garnet porphyroblasts about 0.5 cm in diameter in a well-foliated, biotite-rich matrix spotted with white sillimanite aggregates.

The mineral assemblage contains, in order of decreasing abundance, plagioclase, biotite, fibrolitic sillimanite, garnet, silicate melt, graphite, spinel, ilmenite and K-feldspar; cordierite is absent.

Plagioclase is rich in minute inclusions of glass and/or graphite (Cesare and Maineri 1999); in places it shows a weak concentric zoning with An-richer rims. Rarely, at the contact with interstitial glass, plagioclase may have a thin rim of coalescent euhedral K-feldspar crystallites (< 100 μm in size) growing into the melt. This texture may be an indication of late-stage, K-feldspar crystallization during cooling of the melt after emplacement of the host dacite.

In all xenoliths, most sillimanite is needle-like (fibrolite) and occurs in the form of knots, subspherical or elongated, along the main foliation. In these knots, fibrolite is intimately intergrown with rhyolitic $melt_1$ (Fig. 1; see also Fig. 3 in Cesare et al. 1997). Although textures resemble those described by Grapes (1986), no evidence of mullite was obtained by powder X-ray diffraction of the fibrolite-$melt_1$ aggregate, hereinafter called "mix". Less frequently, fibrolite occurs as inclusions in garnet, biotite or plagioclase. $Melt_1$ is also present in melt inclusions within plagioclase and biotite, and in films or pockets at grain boundaries or junctions.

Garnet is generally euhedral, but in places it shows resorbed grain boundaries at contacts with biotite or melt. It may include biotite, glass and rare quartz, and is often coated by a thin film of glass, in which spinel may be present (Fig. 2).

Biotite lamellae are < 2 mm in size, and are concentrated in decussate layers that outline the foliation. In this habit, biotite is generally fresh, with straight grain boundaries and only minor evidence of reaction to glass and spinel. Textures indicating replacement are more apparent and occur wherever biotite crystals are in contact with (or immersed in) the mix aggregate (Fig. 3). Here, biotite shows resorbed grain boundaries characterized by embayments, and is wrapped by a continuous, < 200-μm-thick reaction rim composed of glass, spinel and ilmenite (Fig. 4). In the reaction rim, spinel forms euhedral, slightly elongate crystals up to 100 μm in size, often intergrown with (and possibly nucleating from) needle-like or dendritic ilmenite (Fig. 5). Spinel and ilmenite are immersed in the glassy matrix (*melt$_2$*) that coats biotite grains and grades towards the mix aggre-

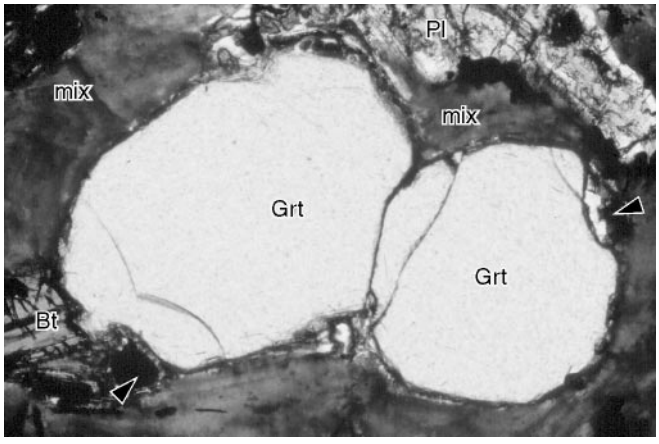

Fig. 2 Garnet porphyroblast with a thin rim of melt and small spinel crystals (*arrows*). Plane-polarized light, width of view 3.5 mm

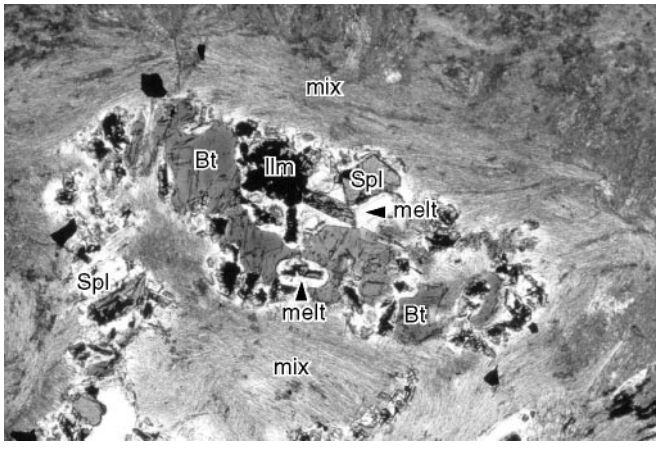

Fig. 3 Photomicrograph of resorbed biotite immersed in the mix aggregate. Embayments of biotite contain melt, spinel and ilmenite. Plane-polarized light, width of view 1.5 mm

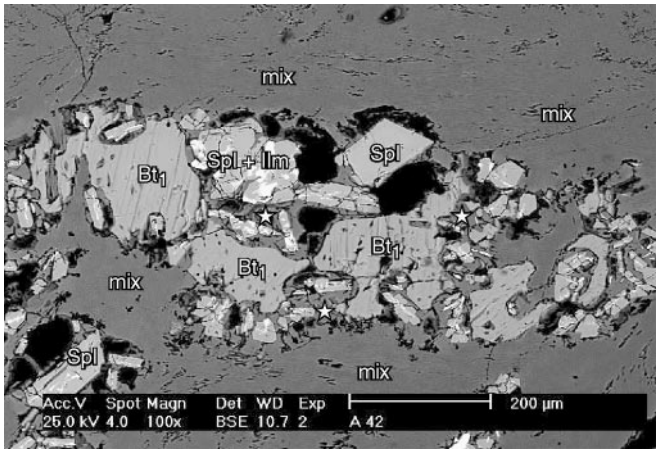

Fig. 4 Backscattered electron (BSE) image of the reaction site of biotite melting. *Stars* indicate $melt_2$ areas

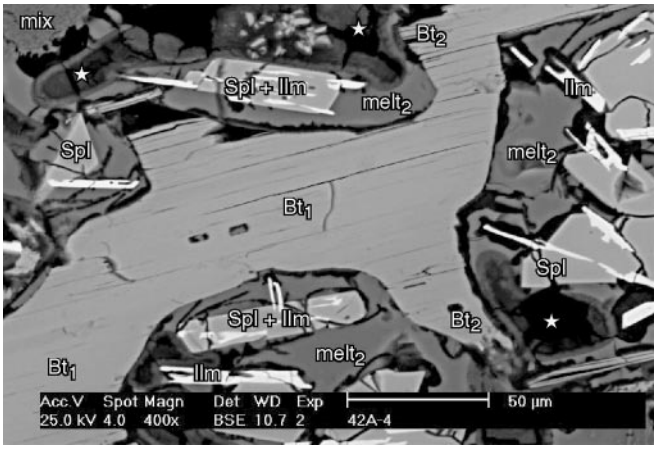

Fig. 5 Detail BSE image of the textures of biotite melting. Resorbed biotite is coated by a continuous rim of $melt_2$ where needle-like ilmenite and euhedral spinel occur. Black round holes (*stars*) result from weathering of altered glass. Small dark spots in biotite are melt inclusions

gate, so that the melt/fibrolite ratio of mix is higher adjacent to biotite. The glass is generally fresh with only minor alteration to very fine-grained brown aggregates containing jarosite (Zeck 1968). These weathered aggregates are weak and erode during sample preparation (see Fig. 5).

Spinel occurs throughout the xenoliths beyond the reaction site, but is not observed as inclusions in garnet. This suggests that spinel growth post-dates crystallization of garnet. Textural analysis of the replacement rim indicates that spinel formation is coeval with that of ilmenite and $melt_2$, and occurs by reaction of biotite with the mix aggregate. Rims of spinel and melt around garnet (Fig. 2) would suggest that garnet might also be involved as a reactant in the production of spinel. The role of plagioclase and K-feldspar is ambiguous, since they do not appear in the reaction texture; the occurrence of K-feldspar away from the sites of biotite melting in association with interstitial melt layers, and its very low abundance, suggests a late stage origin, unrelated to spinel growth.

Phase chemistry

All phases present in the sample were analysed using a Cameca Camebax electron microprobe (EMP) of CNR (Consiglio Nazionale delle Ricerche) at the Department of Mineralogy and Petrology of the University of Padova. Working conditions were 15-kV accelerating voltage and 15-nA sample current; natural and synthetic silicates and oxides were used as standards, and data correction was performed using PAP methods as adapted by Cameca. Table 1 reports sample point analyses of the phases, whereas the description below refers to the full set of EMP analyses, available in the electronic supplementary material. Where relevant, data from sample HO42 are compared with data from similar, Spl-free xenoliths from El Joyazo (Cesare et al. 1997; B. Cesare, unpublished data). The beam diameter was generally focussed to ca. 1 μm; where possible, it was defocussed to ca. 5 μm in the analysis of biotite and glass, and to ca. 5 and ca. 10 μm to obtain an integrated composition of the mix aggregate. In order to avoid loss of Na in glasses, which resulted to be up to 30% relative as a function of the time spent by the beam on the point before and during analysis, Na was analysed as the first element, at 10-nA sample current and 6-s count time, moving to the analysis point immediately before the start of counting. Checked against a glass standard with comparable Na content, this technique shows the concentration of Na to be within 5% relative.

Biotite

Biotite crystals (Bt_1) are homogeneous except for a thin (<20 μm) rim at the contact with $melt_2$ (Bt_2). Bt_1 is aluminous ($Al^{VI} = 0.64$ atoms/22 oxygens), Ti-rich (0.58 atoms), with an average X_{Mg} [$Mg/(Mg + Fe) = 0.35$]. The composition of Bt_1 is almost identical to biotites from other xenoliths at El Joyazo. The rim of Bt_2 has lower Al^{VI} (0.59), higher Ti (up to 0.68 atoms) and X_{Mg} (0.45). Compositional changes from Bt_1 to Bt_2 are in agreement with the field and experimental observations indicating Ti increase, Al^{VI} decrease and a positive Ti/X_{Mg} correlation with increasing temperature (Guidotti 1984; Brearley 1987; Patiño Douce et al. 1993; Patiño Douce and Beard 1996; Stevens et al. 1997). The high Na content of Bt_2 (up to 0.18 atoms) is similar to the values reported by Montel and Vielzeuf (1997).

Spinel

Hercynitic spinel is essentially a binary Fe-Mg mixture, in which the gahnite end-member (Zn) never exceeds 0.016, and other cations such as Cr, Ni and V are present in negligible amounts. Ferric iron contents, estimated by charge balance, are <0.045 atoms, resulting in Fe^{3+}/Fe_{tot} ratios $<6\%$. Spinel has X_{Mg} ranging from 0.22 to 0.34, with systematically lower values in the core of crystals; Zn content decreases from core to rim.

Ilmenite

Fine-grained ilmenite shows constant composition, and is characterized by low Fe^{3+}/Fe_{tot} ($<6\%$), low Mn (<0.01 atoms) and $X_{Mg} = 0.05$.

$Melt_2$

Compositions of $melt_2$ in Table 1 have been normalized to 100% for comparison with other sets of analyses.

Table 1 Sample EMP analyses of all phases from xenolith HO42

Phase	Bt_1	Bt_2	Spl	Spl	Spl	Spl	Ilm	Grt	Grt	Pl_1	Pl_2	Kfs	$Melt_2$	$Melt_2$	mix	mix	mix
Id	bt14	btl1	sp2c (core)	sp2r (rim)	SP8c (core)	sp8r (rim)	ilm3	gtln (core)	gt1c (rim)	pl6c	pl6a	Kfs1	ve4	ve8	mix1	mix5	mix9
Al_2O_3	18.94	18.26	60.06	61.01	58.77	60.01	0.56	21.01	21.15	25.23	27.11	19.61	15.29	15.44	42.85	47.03	51.96
CaO	0.00	0.05	0.00	0.00	0.00	0.00	0.09	3.19	0.92	6.56	8.96	0.41	1.03	1.18	0.44	0.32	0.28
Cr_2O_3	0.06	0.03	0.18	0.04	0.09	0.09	0.03								0.03	0.04	0.02
Fe_2O_3			1.41	0.96	1.98	2.18											
FeO	21.76	19.09	30.68	28.77	32.73	31.74	45.60	34.07	36.31	0.01	0.10	0.09	1.25	1.24	0.68	0.59	0.44
K_2O	8.44	8.79	0.00	0.02	0.03	0.01	0.03	0.00	0.01	0.92	0.81	11.60	6.00	6.08	2.31	1.75	1.36
MgO	6.42	8.70	6.97	8.51	5.34	6.62	1.47	2.51	3.09	0.00	0.00	0.00	0.16	0.12	0.11	0.05	0.04
MnO	0.00	0.02	0.10	0.00	0.06	0.02	0.34	2.52	1.46	0.05	0.00	0.01	0.00	0.03	0.02	0.00	0.04
Na_2O	0.30	0.60	0.00	0.04	0.01	0.01	0.00	0.04	0.00	7.28	6.23	2.90	3.79	2.59	1.54	0.96	0.88
SiO_2	34.41	34.98	0.03	0.04	0.11	0.05	0.08	37.38	37.67	60.72	57.60	65.03	72.20	73.10	51.87	48.54	44.85
TiO_2	5.11	6.00	0.33	0.35	0.37	0.30	50.71	0.00	0.03	0.01	0.04	0.03	0.28	0.23	0.11	0.07	0.08
ZnO	0.00	0.00	0.47	0.14	0.78	0.31											
H_2O[a]													3.33	4.37			
Total	95.43	96.53	100.23	99.89	100.29	101.35	98.90	100.73	100.64	100.77	100.85	99.69	100.00	100.00	99.96	99.35	99.94
Si^{IV}	5.276	5.253															
Al^{IV}	2.724	2.747															
Al^{VI}	0.698	0.485															
Ti	0.589	0.678	0.007	0.007	0.008	0.006	0.960	0.000	0.002	0.000	0.001	0.001					
Cr	0.007	0.003	0.004	0.001	0.002	0.002	0.001										
Fe^{2+}	2.790	2.398	0.708	0.658	0.767	0.728	0.898										
Mn	0.000	0.003	0.002	0.000	0.002	0.001	0.007	0.171	0.099	0.002	0.000	0.001					
Mg	1.467	1.947	0.287	0.347	0.223	0.271	0.055	0.300	0.369	0.000	0.000	0.000					
O site	5.551	5.513															
Ca	0.000	0.008	0.000	0.000	0.000	0.000	0.000	0.274	0.079	0.311	0.428	0.020					
Na	0.088	0.176	0.000	0.000	0.000	0.000	0.000	0.006	0.000	0.625	0.539	0.257					
K	1.650	1.684	0.000	0.000	0.000	0.000	0.000	0.000	0.001	0.052	0.046	0.674					
A site	1.739	1.868															
Al			1.953	1.965	1.941	1.941	0.016	1.984	1.995	1.316	1.424	1.053					
Fe								2.283	2.429	0.000	0.004	0.004					
Fe^{3+}[b]			0.029	0.020	0.042	0.045	0.062										
Si			0.000	0.000	0.000	0.000	0.001	2.996	3.014	2.687	2.568	2.964					
Zn			0.010	0.003	0.016	0.006											
Alm								0.75	0.82								
Sps								0.06	0.03								
Pyp								0.10	0.12								
Grs								0.09	0.03								
Ab										0.63	0.53	0.27					
An										0.32	0.42	0.02					
Or										0.05	0.05	0.71					
Crn-n													0.65	2.36			
A/CNK													1.18	1.30			
X_{Mg}	0.34	0.45	0.28	0.34	0.22	0.026	0.06	0.12	0.13				0.18	0.15	0.22	0.13	0.13
Oxygens	22	22	4	4	4	4	3	12	12	8	8	8					

[a] Reported H_2O value corresponds to 100 − EMP closure value
[b] Fe^{3+} in spinel and ilmenite recalculated by charge balance

Although it represents only a first order, overestimated approximation, the difference between 100% and the sum of all analysed oxides is assumed to represent the H_2O content of the glass and is also reported. The melt is rhyolitic, felsic (FeO + MgO + TiO_2 < 1.65 wt%), peraluminous (Al_2O_3/(CaO + Na_2O + K_2O) > 1.11) and inferred to be hydrous. The restricted variations of the three major components SiO_2, Al_2O_3 and K_2O indicate that $melt_2$ is homogenous, although notable variations are observed for Na_2O (from 2.5 to 3.8 wt%) and X_{Mg} (from 0.12 to 0.22). Compared to glasses analysed in other xenoliths (E. Salvioli Mariani, unpublished data), $melt_2$ in sample HO42 has higher Al_2O_3, CaO and Na_2O + K_2O, and lower SiO_2, defining an independent field in the CIPW normative Qtz-Ab-Or diagram of Fig. 6. These chemical variations are in agreement with the trends of Al, Ca and alkali enrichment observed with increasing T in experimental runs (Ellis 1986; Patiño Douce and Johnston 1991; in part Holtz and Johannes 1991 and Stevens et al. 1997) and confirm that the orthoclase component of decomposing biotite enters the melt (Vielzeuf and Montel 1994), whereas Fe, Mg and Ti are buffered to very low values by partitioning into spinel and ilmenite. However, the above experiments do not reproduce the biotite melting reaction considered in this paper, and hence extrapolation of their results, which were obtained from different chemical systems, should be considered with caution.

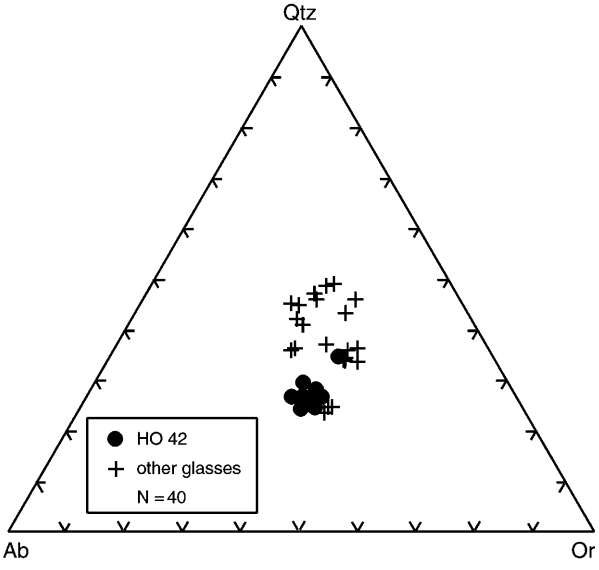

Fig. 6 CIPW normative Qtz-Ab-Or triangle showing $melt_2$ compositions of sample HO42 (*filled circles*) and other xenoliths of El Joyazo (*crosses*). $Melt_2$ produced by the breakdown of biotite is clearly more alkaline and contains less silica

Mix

Large chemical variations are intrinsic in the two-phase nature of the mix aggregate. The relationships between SiO_2 and Al_2O_3 (Fig. 7) clearly demonstrate that mix compositions are linear combinations of an Al_2SiO_5 component (fibrolite, because mullite was not detected) and a rhyolitic $melt_1$ in proportions that vary from ca. 25 wt%–ca. 40 wt% melt. The calculated average mix in Table 2 corresponds to a fibrolite:$melt_1$ ratio of ca. 2:1. It is also apparent that the $melt_1$, intermixed with sillimanite in the mix aggregate, is different from the melts analysed both in the reaction rim ($melt_2$) and in other xenoliths because these plot away from the extrapolated mixing line. Despite the compositional variability, values of X_{Mg} in the mix are restricted to the range 0.13–0.22, overlapping with those of the $melt_2$ phase.

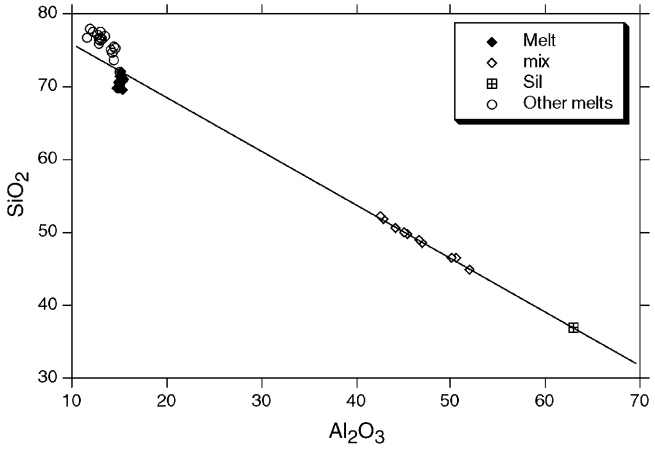

Fig. 7 SiO_2 vs. Al_2O_3 diagram illustrating the relationships between composition of stoichiometric sillimanite (*square*), and EMP compositions of mix (*open diamonds*) and $melt_2$ (*filled diamonds*). Also reported are other glass analyses from similar Grt-Bt-Sil xenoliths (*circles*). Alignment between mix and sillimanite demonstrates the two-phase ($melt_1$ + fibrolite) nature of the mix that justifies its large chemical variations. The departure of melt compositions from the visually extrapolated mixing line shows that the composition of $melt_1$ in the mix aggregate differs from that of intergranular fluid film and melt inclusions

Garnet

Garnet is slightly zoned with a composition continuously changing from a Ca- and Mn-richer core ($Alm_{75}Pyp_{10}Sps_{06}Grs_{09}$) to a rim closer to a Fe-Mg solution ($Alm_{82}Pyp_{12}Sps_{03}Grs_{03}$). Values of X_{Mg} change from 0.12 in the core to 0.14 at the rim.

Plagioclase

Plagioclase shows a zoning pattern characterized by large, homogeneous cores (Pl_1) surrounded by a more calcic rim (Pl_2) about 50 μm thick. The increase of anorthite from 31% in Pl_1 to 49% in Pl_2 is consistent with experimental data on plagioclase evolution during melting of biotite in Pl-bearing systems (e.g. Patiño Douce and Harris 1998; Stevens et al. 1997); on the other hand, simultaneous enrichment in K is not observed in the studied example, where the K-feldspar content of plagioclase is slightly decreasing (5–4%). The composition of Pl_1 is the same as that measured in all other xenoliths (Cesare et al. 1997).

K-feldspar

The rare K-feldspar occurring as intergrowths with plagioclase or as thin rims at the contact plagioclase-melt has composition $Or_{71}Ab_{27}An_{02}$.

Fe-Mg partitioning

As concerns the Fe-Mg partitioning, the histograms of Fig. 8 summarize X_{Mg} relationships among phases analysed, consistently arranged in the sequence: $Bt_2 > Bt_1 > Spl > melt_2 = mix \geq Grt > Ilm$. Also reported in Fig. 8 is the range of X_{Mg} of Grt-Bt-Sil xenoliths of El Joyazo, which is 0.20–0.27 (G. Venturelli, unpublished data). The lowest X_{Mg} values (ca. 0.15) of $melt_2$ and mix overlap those of garnet. These relationships and their implications are discussed in the next section.

Modelling biotite melting

Mass balance relationships

The development of reaction rims between biotite and mix suggests a melting reaction that involves Spl, Ilm

Table 2 Input matrices of data (average of n EMP analyses) and errors (1σ standard deviation) used in the mass balance calculation. Atoms in melt and mix were calculated on the basis of 10 oxygens

Phase	Bt_1	Pl_1	mix	Grt	Ilm	$melt_2$	Bt_2	Spl	Pl_2
No. of points	9	8	9	3	3	10	16	20	6
a) Data									
Al	3.361	1.298	1.494	1.992	0.009	0.502	3.332	1.954	1.475
Ca	0.005	0.306	0.011	0.084	0.000	0.031	0.005	0.000	0.488
Fe	2.814	0.003	0.013	2.428	0.955	0.027	2.394	0.754	0.006
K	1.659	0.050	0.066	0.001	0.000	0.207	1.642	0.000	0.038
Mg	1.505	0.001	0.003	0.386	0.053	0.005	1.937	0.271	0.001
Mn	0.007	0.001	0.001	0.081	0.007	0.001	0.004	0.002	0.000
Na	0.102	0.633	0.068	0.005	0.000	0.195	0.143	0.000	0.472
Si	5.282	2.700	1.333	3.015	0.001	1.987	5.261	0.000	2.517
Ti	0.585	0.001	0.002	0.001	0.971	0.004	0.602	0.007	0.001
b) 1σ errors									
Al	0.039	0.018	0.108	0.013	0.007	0.007	0.052	0.014	0.060
Ca	0.005	0.017	0.003	0.004	0.001	0.003	0.006	0.001	0.061
Fe	0.100	0.003	0.002	0.026	0.009	0.002	0.051	0.041	0.003
K	0.030	0.004	0.013	0.004	0.001	0.008	0.034	0.001	0.007
Mg	0.083	0.001	0.001	0.015	0.002	0.002	0.057	0.040	0.001
Mn	0.005	0.001	0.001	0.016	0.002	0.001	0.004	0.001	0.001
Na	0.011	0.022	0.017	0.005	0.001	0.022	0.017	0.001	0.055
Si	0.022	0.017	0.073	0.004	0.001	0.008	0.035	0.001	0.060
Ti	0.010	0.001	0.001	0.001	0.014	0.001	0.029	0.002	0.001

and $melt_2$ as products. As with many corona textures, it is also possible that such a reaction ceased as a consequence of a mantling of reactant(s) by stable product phase(s), so that conditions of mosaic equilibrium were attained. As the chemical composition of all phases present in the rock has been characterized in detail, it should be possible to calculate or infer a mass balance that describes the melting reaction, or represents a close approximation to it. To do this, the most appropriate and sufficiently constrained chemical system, and the phases to be modelled with it, must be defined.

Because the reaction texture contains biotite, spinel, ilmenite, mix and $melt_2$, the model system must include SiO_2, Al_2O_3, FeO_{tot}, MgO, K_2O, H_2O, Na_2O, CaO and TiO_2, all present in relevant amounts in at least one phase. Modelling of Na_2O and CaO requires consideration of plagioclase and garnet, which may have been involved in the melting of biotite even if they occur away from the reaction site. In turn, garnet adds the component MnO to the system, which finally becomes a natural "pelitic" KFMASH-Ti-Ca-Na-Mn.

The nine components define the rows of an input matrix (Table 2a) where the columns represent the analysed phases. The mass balance calculations consider nine phases – Bt_1, Bt_2, Spl, Ilm, $melt_2$, mix, Pl_1, Pl_2 and Grt_{rim} – expressed as average values of n spot analyses, using the approach described by Fisher (1989). Table 2b is the error matrix, containing the estimated analytical uncertainties (1σ standard deviation of the average values) to be used in the evaluation of adequacy of model matrices. K-feldspar was not included in the input matrices because textural analysis suggests it did not participate in the melting reaction.

By definition, a full rank nine-by-nine matrix cannot define mass balance relationships, unless the number of independent compositional parameters, its rank, is actually lower. This can be evaluated by reducing the rank of the input matrix (Fisher 1989), and then assessing the adequacy of the resulting model matrix by means of the error matrix (see Hartel and Pattison 1996; Cesare 1999). Reduction of matrix rank to eight generates an acceptable model in which only three error ratios are >1 (1.6, 1.9 and 1.1) related to the Mn component of Bt_1, $melt_2$ and Bt_2. The reduced model matrix defines one mass balance, expressed in mole units as:

$$0.78Bt_1 + 1.95Pl_1 + 2.82mix + 0.32Grt = 0.25Ilm + 5.00melt_2 + 0.30Bt_2 + 2.53Spl + 1.03Pl_2 \quad (1)$$

and in weight units as:

$$4.3Bt_1 + 3.0Pl_1 + 2.7mix + 0.9Grt = 0.2Ilm + 5.0melt_2 + 1.6Bt_2 + 2.4Spl + 1.6Pl_2 \quad (1a)$$

This mass balance represents an intersection of tielines in the eight-component composition space, and can be interpreted as an univariant reaction, or as evidence of disequilibrium of one or more phases (Fisher 1989). In the present case the agreement with the observed textures, represented by the match of phases in their inferred role of reactants or products, suggests that the mass balance relationship is a suitable model for the natural reaction of biotite melting. As the mass balance relates phases (Bt, Pl, melt) with markedly different composition on either side, the melting reaction must be interpreted as a disequilibrium reaction.

The matrix analysis has been performed also using two garnet compositions (core and rim), but it failed to reproduce the observed textures, because the resulting mass balance of ten phases in the nine-component system contained Grt_{rim} as the reactant and Grt_{core} as the product. In this case, rank reduction of the ten-by-nine matrix was not possible owing to the very large errors related to the Mn component.

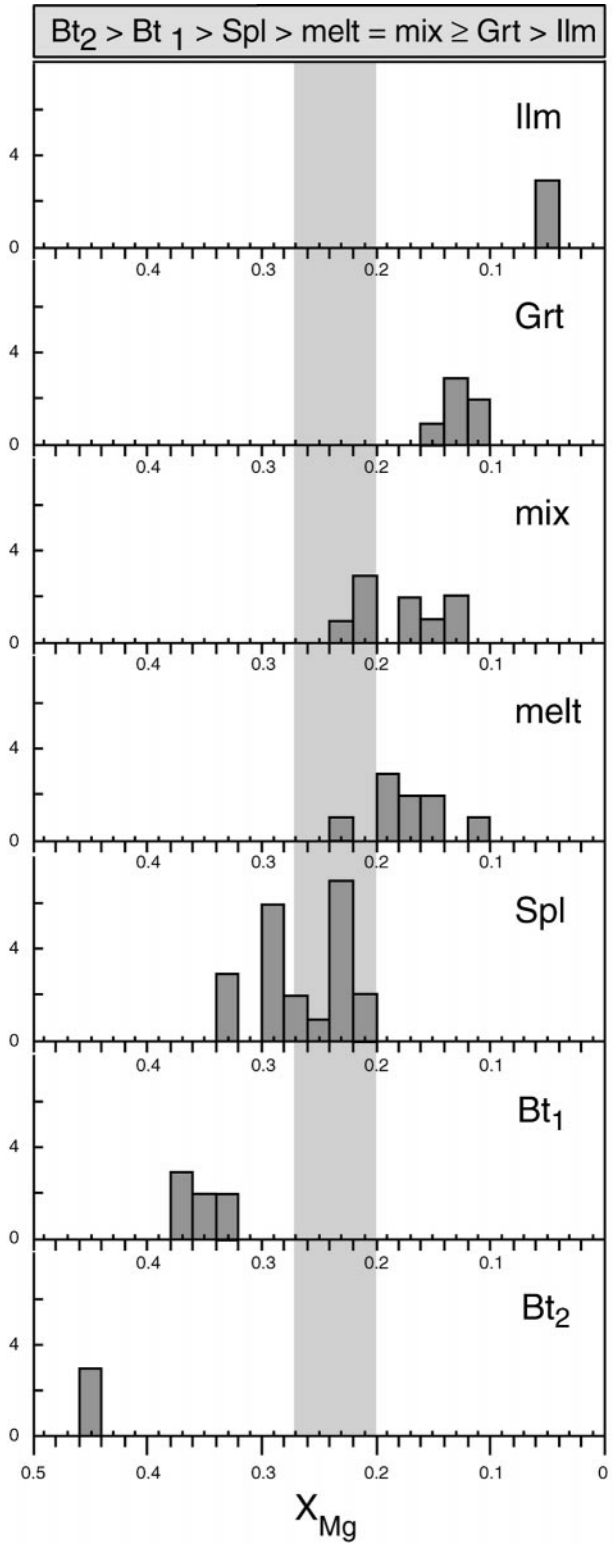

Fig. 8 Combined X_{Mg} histogram of the Fe-Mg phases of sample HO42. See text for details

P-T conditions

The *P-T* conditions at which biotite melting occurred can be constrained by use of conventional thermobarometers, but the results show a large scatter. The garnet-biotite thermometer of Ferry and Spear (1978) applied to Grt_{rim}-Bt_2 pairs yields *T* values generally < 600 °C, whereas Grt_{rim}-Bt_1 pairs yield values in the range 750–800 °C. The Grt-Ilm thermometer of Pownceby et al. (1987) gives $T = 740$ °C. These results are inconsistent with the phase assemblage, and with independent indications on the high temperatures attained in similar xenoliths during partial melting (Cesare et al. 1997). As concerns the Grt-Bt thermometry, this method has been successfully applied to very high temperatures in natural and experimental assemblages (Indares and Martignole 1985; Le Breton and Thompson 1988; Stevens et al. 1997). Furthermore, it can be also observed that the Grt-Bt temperatures obtained in all other xenoliths free of Bt-melting textures (Cesare et al. 1997), fall in the "reasonable" interval 800–900 °C. The indicated Grt-Bt temperatures in sample HO42 are likely caused by disequilibrium between garnet and Bt_2.

GASP barometry (Newton and Haselton 1981), using Pl_2 and $Grt_{rim,}$ yields maximum pressures (since quartz is absent) from 2.8 kbar (at 800 °C) to 4.7 kbar (at 950 °C). These values are strongly dependent on calibration: the calibration of Hodges and Spear (1982), using identical assemblage in the same *T* interval, provides a *P* range of between 1.1 and 2.2 kbar. The Grt_{rim}-Pl_2-Bt_2-Qtz barometer of Hoisch (1990) yields a similar pressure interval of 3.4 kbar (at 800 °C) to 4.5 kbar (at 950 °C). These pressure values are lower than those obtained by Cesare et al. (1997). However, the possibility of garnet disequilibrium, and its bearing on the (lack of) significance of these estimates should be taken into account, also considering the low grossular content.

An alternative approach to *P-T* evaluation is comparison with experimentally calibrated equilibria in the pelitic system. As concerns temperature, the Ti content of Bt_2 is as high as (or higher than) maximum values measured in experiments of biotite melting (Patiño Douce and Johnston 1991; Patiño Douce et al. 1993; Gardien et al. 1995; Patiño Douce and Beard 1996; Stevens et al 1997, all coexisting with a Ti-saturating phase) at temperatures in the range 900–950 °C. A similar indication is provided by chemical relationships between garnet and $melt_2$: the partial overlap of X_{Mg} values (average garnet being Fe-richer than average $melt_2$) indicates an approach to unity of $K_D^{Grt\text{-}melt}$. These conditions, i.e. the reversal of the garnet-liquid Fe-Mg relationships, have been observed at ≈900 °C by Ellis (1986) and ≈950 °C by Vielzeuf and Holloway (1988). Based on this good agreement with most of the available experimental data, it is suggested that temperatures during biotite melting to spinel were in the range 900–950 °C.

Independent constraints on pressure are poor. The lack of cordierite or the textural indications of garnet persistence would be in agreement with minimum pressures of about 5 kbar (Patiño Douce and Beard 1996), but better precision is necessary.

Role of H_2O

Although present, the H_2O component is not considered in the model system and in mass-balance calculations because it was not directly measured in the biotite, glass and mix phases, and because the values inferred from EMP closure values or determined by stoichiometry may be affected by large uncertainties. Omission of the H_2O component is "legal" when an aqueous fluid is present in the system; however, in the present case, petrographic observation does not constrain the role of fluids during biotite melting.

The role of this component can be evaluated if the H_2O content of reactants Bt_1 and mix is sufficient to balance that of products Bt_2 and $melt_2$ in the mass balance, or if a free aqueous phase needs to be present. Using $melt_2$ average H_2O contents (3.5 wt%) as inferred from EMP totals, products would require about 25% H_2O in excess of that released by reactants. As the H_2O contents deduced by EMP closure values are probably overestimated (e.g. Ellis 1986), the minimum value (2.0 wt%) was also used instead of the average. In this case a good balance was obtained. Because further uncertainty can be introduced by non-stoichiometry in the OH content of biotite (i.e. dehydroxylation mechanisms, Bohlen et al. 1980), it can be concluded that the role of H_2O cannot be constrained by mass balance with the available data, as conflicting answers are available.

Note that the (overestimated) H_2O content of $melt_2$ is much lower than the saturation range for rhyolitic melts (Holtz et al. 1995) at the *P-T* values inferred above; conversely, it is close to the values expected for melts generated at low a_{H_2O} (e.g. Vielzeuf and Montel 1994). This suggests that an aqueous fluid phase was not in excess during melting, and that the process was fluid-absent. Although more, definitive constraints are needed, such a conclusion seems reasonable considering that extensive anatexis, producing H_2O-undersaturated melts, had already occurred in the xenoliths, and that there is no evidence for low-a_{H_2O} fluids trapped in fluid inclusions.

Discussion

High-*T* exchange mechanisms in biotite

As Al^{IV} and Si do not show appreciable variations from Bt_1 to Bt_2, the relevant changes in the composition of biotite during melting are restricted to the octahedral site, involving Al^{VI}, Ti, Fe and Mg. The chemical data obtained in this study are projected in the binary plots of Fig. 9 with other biotite compositions from similar xenoliths, allowing evaluation of the possible exchange mechanisms that occurred in the octahedral position.

The diagram of Fig. 9a indicates that the vacancy-forming $TiFe_{-2}$ substitution proposed by Patiño Douce (1993) and Patiño Douce et al. (1993) is not applicable to the biotites of the present study. As the change from Bt_1 to Bt_2 is characterized by an Fe + Mg sum within ±0.05 cations (Fig. 9b), the concentration of Ti must be negatively correlated with that of Al^{VI}: Fig. 9c shows that this correlation exists, and has a trend similar to that suggested by Stevens et al. (1997). However, this correlation is mainly observed in biotites of sample HO42, whereas most biotites from other Spl-free

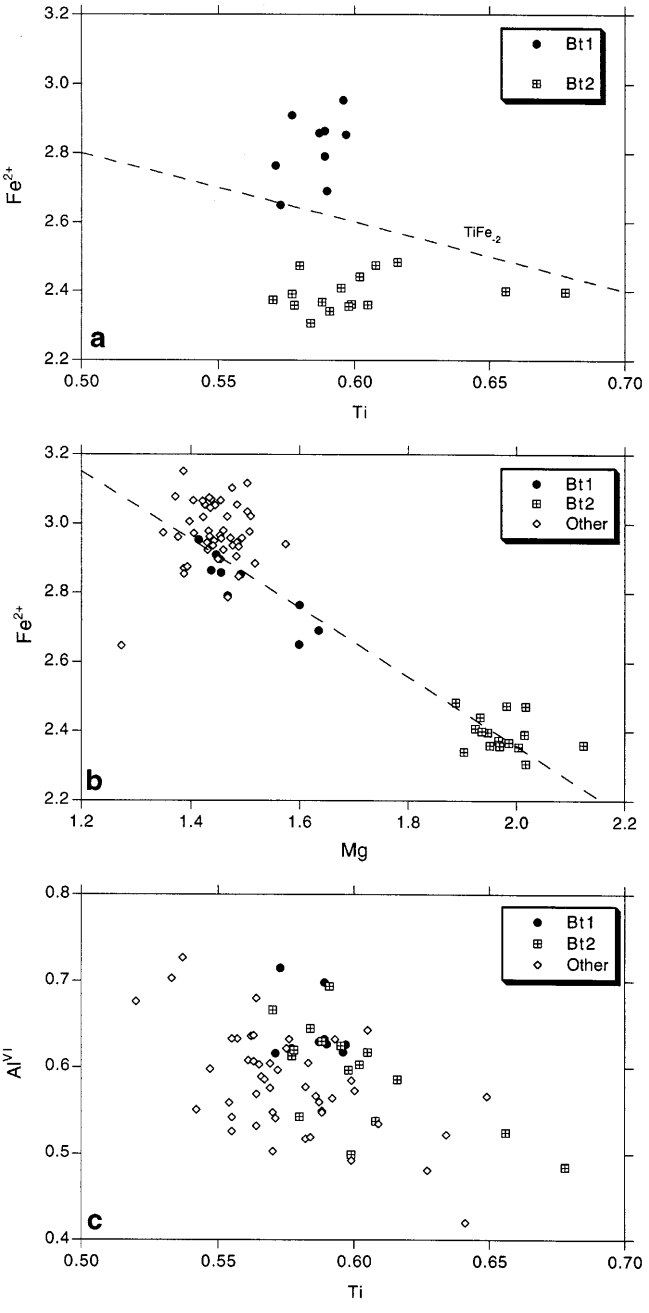

Fig. 9a–c Binary plots illustrating crystal-chemical features of biotite. **a** Fe^{2+} vs Ti diagram: variations from Bt_1 (*filled circles*) to Bt_2 (*squares*) are not consistent with the $TiFe_{-2}$ substitution that would follow a trend parallel to the *dashed line*; **b** Fe^{2+} vs Mg diagram: Bt_1 and Bt_2 have a Fe + Mg sum of 4.35 (*dashed line*) ±0.05 atoms. Biotites from other xenoliths (*empty diamonds*) generally have higher Fe + Mg; **c** Al^{IV} vs Ti diagram: a general negative correlation is apparent only from the data points of Bt_1 and Bt_2, whereas biotites from other xenoliths are more scattered

xenoliths exhibit a different behaviour, characterized by relevant Al^{VI} variations at rather constant Ti. This probably suggests a substitution mechanisms intervening only during melting of biotite in the presence of a phase such as spinel. As both Bt_1 and Bt_2 contain constant Al^{IV}, it is apparent that the Tschermak exchange cannot describe the variations of Al^{VI} and that, as noted by Indares and Martignole (1985) and Brearley (1987), an alternative mechanism for Al^{VI} exchange is needed. Thus, the high-T change from Bt_1 to Bt_2 seems to be a coupled mechanism of octahedral substitution, represented by the simultaneous Ti-Al exchange and $MgFe_{-1}$ substitution. It is important to bear in mind that the above discussion relies on the scheme of biotite normalization to 44 negative charges. This implicitly and arbitrarily excludes the occurrence of the Ti-oxy substitution (e.g. Cruciani and Zanazzi 1994, Dyar et al. 1993), which can be evaluated only by direct measurement of Fe^{3+} and OH content.

Biotite melting reaction

The mass balance obtained in this study resembles the biotite fluid-absent melting reaction proposed by Stevens et al. (1997):

$$Bt + Qtz + Pl_1 + Sil = Kfs \pm Grt \pm Crd + melt + Pl_2 \pm Ilm \quad (2)$$

in which it is shown that plagioclase changes composition during melting. The main difference with this and other biotite melting reactions proposed for metapelites (see also Le Breton and Thompson 1988; Vielzeuf and Holloway 1988; Patiño Douce and Johnston 1991) is the absence of quartz as a reactant (and of K-feldspar as a product), which causes spinel formation and a reverse role for garnet (or cordierite, depending on pressure), which in the present case study is a reactant. Based on Schreinemakers analysis in the simplified system KFASH, Montel et al. (1986) proposed the melting reaction:

$$Bt + Sil + Grt + vapour = Spl + melt \quad (3)$$

This Qtz-absent reaction predicts garnet as reactant (e.g. Grant 1985) and does not contain K-feldspar, but is fluid-present.

Modelling of biotite melting in natural metapelites generally requires consideration of the non-KFMASH components Na, Ca, Ti and occasionally Mn. The addition of these components results in the presence of one extra Ca-Na phase, plagioclase, and possibly one extra Ti-phase (ilmenite or rutile as a function of pressure). When ilmenite is not stable, Mn and Ti are strongly partitioned into garnet and biotite, respectively. As a result of the relationships between extra components and extra phases it follows that, unless the bulk system has an anomalous or degenerate composition, most univariant melting equilibria proposed for the model pelitic system (e.g. Grant, 1985) – or even for the CNKFMASH system (Spear et al. 1999) – are indeed at least divariant.

The mass balance obtained in this study can be rewritten as:

$$Bt_1 + Pl_1 + Sil + melt_1 + Grt = Ilm + melt_2 + Bt_2 + Spl + Pl_2 \quad (1b)$$

Although this might indicate a univariant reaction in a model system with eight compositional degrees of freedom, it has been already pointed out how it actually involves, as both reactants and products, three phases with distinct composition (biotite, plagioclase and melt). It follows that the mass balance represents a disequilibrium reaction, although it relates P-T conditions that are relatively close to each other: 850 ± 50 °C and 5–7 kbar before biotite melting (Cesare et al. 1997), 900–950 °C and ≈5 kbar during biotite melting (this study). It is suggested that this disequilibrium reaction approximates the continuous reaction by which biotite would melt under equilibrium conditions. In this perspective, because the real number of phases involved is seven, the continuous reaction would be trivariant. Note that the variance would be increased by one in the likely case that the system was fluid-absent.

Support for biotite melting in high variance assemblages, i.e. over a large (isobaric) temperature interval, is found in most experimental studies that use natural or complex synthetic starting materials of bulk compositions ranging from pelite to greywacke, at variable Al saturation and contents of "extra" components Ca, Na, and Ti. All this evidence indicates that di- or multivariant biotite melting is to be expected as the rule in natural rocks, and not only in the presence of a TiO_2 component. The major effects of minor components on the stability of biotite indicate that the KFMASH pelitic system is oversimplified for modelling crustal melting and unsuitable for thermobarometric purposes. The system should be generally considered a starting point for first-order, qualitative analysis.

The involvement of garnet and plagioclase as reactants in mass balance (Eq. 1) indicates that although spinel presence is mainly confined to the narrow reaction zone around biotite, the equilibration volume for the melting reaction extends for at least 1 cm, the average distance between garnet porphyroblasts and reaction sites. It also suggests that textural development was initially controlled by nucleation kinetics: nucleation of products spinel and ilmenite occurred mainly at the surface-$melt_2$ interfaces of melting biotite, where Fe, Mg, Al, and especially Ti were readily available. Reaction progress then became diffusion controlled, and the rate-limiting step was intracrystalline diffusion in zoned plagioclase and biotite, rather than diffusion via the intergranular film of melt. The latter was in fact efficient in transferring mass (Fe, Mg, Ca, Na) from garnet and plagioclase to the reaction site and vice-versa. The mass balance relationship also suggests that melt production was dominated by the availability of K from biotite, whereas Ca and Na were able to move from other sites

to the Bt-controlled reaction interface. This perspective reinforces the interpretation that the rare K-feldspar, absent in the vicinity of biotite, was not participating in the melting reaction.

Melt productivity and composition

Mass balance (Eq. 1a) can be rewritten in weight units in the equivalent form

$$4.3\ Bt_1 + 3.0\ Pl_1 + 0.9\ melt_1 + 1.8\ Sil + 0.9\ Grt = 0.2\ Ilm + 5.0\ melt_2 + 1.6\ Bt_2 + 2.4\ Spl + 1.6\ Pl_2 \quad (1c)$$

where mix has been expressed as 1/3 $melt_1$ + 2/3 Sil. The potential bulk ($melt_2$–$melt_1$) melt productivity of this reaction is 37%, a fairly large proportion for a Qtz-absent system.

The $melt_2$ produced during biotite melting is leucogranitic: silica-rich, corundum normative, and leucocratic; its composition is similar to that of natural peraluminous leucogranitic suites (references cited in Montel and Vielzeuf 1997) and also to melts obtained by experimental fluid-absent melting of metapelitic sources (e.g. Vielzeuf and Holloway 1988; Stevens et al. 1997; Patiño Douce and Harris 1998) and metagreywackes (Montel and Vielzeuf 1997; Patiño Douce and Beard 1996). Note, however, that all experiments on biotite melting done so far have been in Qtz-saturated systems, generally (much) more magnesian than the xenoliths considered in this work, that have $X_{Mg} = 0.20$–0.27.

Thus, the present data extend the experimental constraints to include Qtz-absent, Fe-rich systems, and confirm that biotite melting can produce leucogranitic (FeO < 2 wt%) melts buffered to a fairly constant composition:

- over a wide temperature range: from ≈750 to ≈950 °C
- in a wide range of bulk compositions and degrees of saturation of silica and alumina, i.e.
- with a variable restitic assemblage, characterized in turn by one or more of the phases Grt, Crd, Spl, Opx.

The data also confirm the observations of Stevens et al. (1997) on the stabilizing effect of Ti on biotite, again extending them to iron-richer compositions.

Acknowledgements I wish to thank J. Connolly, C.V. Guidotti, L. Kriegsman, M. Mezzaroba and J-M. Montel for discussion and critical reading of the manuscript, and S. Harley and F. Holtz for their reviews. I acknowledge the help of S. Meli for chemical analysis of melts, of P. Guerriero for SEM imaging and particularly of R. Carampin for EMP analysis. Financial support was given by the University of Padova, Fondi Progetti Ricerca 1998.

References

Bohlen SR, Peacor DR, Essene EJ (1980) Crystal chemistry of a metamorphic biotite and its significance in water barometry. Am Mineral 65: 55–62

Brearley AJ (1987) A natural example of the disequilibrium breakdown of biotite at high temperature; TEM observations and comparison with experimental kinetic data. Min Mag 51: 93–106

Carrington DP, Harley SL (1995) Partial melting and phase relations in high-grade metapelites: an experimental petrogenetic grid in the KFMASH system. Contrib Mineral Petrol 120: 270–291

Cesare B, Salvioli Mariani E, Venturelli G (1997) Crustal anatexis and melt segregation in the restitic xenoliths at El Hoyazo (SE Spain). Mineral Mag 61: 15–27

Cesare B, Maineri C (1999) Fluid-present anatexis of metapelites at El Joyazo (SE Spain): constraints from raman spectroscopy of graphite. Contrib Mineral Petrol 135: 41–52

Cesare B (1999) Multi-stage pseudomorphic replacement of garnet during polymetamorphism: 2. Algebraic analysis of mineral assemblages. J Metamorphic Geol 17: 735–746

Cruciani G, Zanazzi P-F (1994) Cation partitioning and substitution mechanisms in 1 M phlogopite; a crystal chemical study. Am Mineral 79: 289–301

De Larouziere FD, Bolze J, Bordet P, Hernandez J, Montenat C, Ott d'Estevou P (1988) The betic segment of the lithospheric Trans-Alboran shear zone during the late Miocene. Tectonophysics 152: 41–52

Dyar M, Guidotti CV, Holdaway MJ, Colucci M (1993) Nonstoichiometric hydrogen contents in common rock-forming hydroxyl silicates. Geoch Cosmoch Acta 57: 2913–2918

Ellis DJ (1986) Garnet-liquid Fe^{2+}-Mg equilibria and implications for the beginning of melting in the crust and subduction zones. Am J Sci 286: 765–791

Ferry JM, Spear FS (1978) Experimental calibration of the partitioning of Fe and Mg between biotite and garnet. Contrib Mineral Petrol 66: 113–117

Fisher GW (1989) Matrix analysis of metamorphic mineral assemblages and reactions. Contrib Mineral Petrol 102: 69–77

Fitzsimons ICW, Harley SL (1994) The influence of retrograde cation exchange on granulite P-T estimates and a convergence technique for the recovery of peak metamorphic conditions. J Petrol 35: 5432–576

Gardien V, Thompson AB, Grujic D, Ulmer P (1995) Experimental melting of biotite + plagioclase + quartz ± muscovite assemblages and implications for crustal melting. J Geophys Res 100: 15581–15591

Grant JA (1985) Phase equilibria in partial melting of pelitic rocks. In: Ashworth JR (ed) Migmatites. Blackie and Son 86–144

Grapes RH (1986) Melting and thermal reconstitution of pelitic xenoliths, Wehr volcano, East Eifel, West Germany. J Petrol 27: 343–396

Guidotti CV (1984) Micas in metamorphic rocks. In: Bailey SW (ed) Micas. (Reviews in Mineralogy, 13) Mineral Soc Am, Washington, DC, pp 357–468

Harris N (1981) The application of spinel-bearing metapelites to *P*/*T* determinations: an example from south India. Contrib Mineral Petrol 76: 229–233

Hartel THD, Pattison DRM (1996) Genesis of the Kapuskasing (Ontario) migmatitic mafic granulites by dehydration melting of amphibolite: the importance of quartz to reaction progress. J Metamorphic Geol 14: 591–611

Hodges KV, Spear FS (1982) Geothermometry, geobarometry and the Al2SiO5 triple point at Mt. Moosilauke, New Hampshire. Am Mineral 67: 1118–1134

Hoisch TD (1990) Empirical calibration of six geobarometers for the mineral assemblage quartz + muscovite + biotite + garnet. Contrib Mineral Petrol 104: 225–234

Holtz F, Johannes W (1991) Genesis of peraluminous granites. I. Experimental investigation of melt compositions at 3 and 5 kbar and various H_2O activities. J Petrol 32: 935–957

Holtz F, Behrens H, Dingwell DB, Johannes W (1995) Water solubility in haplogranitic melts. Compositional, pressure and temperature dependence. Am Mineral 80: 94–108

Indares A, Martignole J (1985) Biotite-garnet geothermometry in the granulite facies: the influence of Ti and Al in biotite. Am Mineral 70: 272–278

Kretz R (1983) Symbols for rock-forming minerals. Am Mineral 68: 277–279

Kriegsman LM, Hensen BJ (1998) Back reaction between restite and melt: implications for geothermobarometry and pressure-temperature paths. Geology 26: 1111–1114

Le Breton N, Thompson ABT (1988) Fluid-absent (dehydration) melting of biotite in metapelites in the early stages of crustal anatexis. Contrib Mineral Petrol 99: 226–237

Montel J-M, Weber C, Pichavant M (1986) Biotite-sillimanite-spinel assemblages in high-grade metamorphic rocks: occurrences, chemographic analysis and thermobarometric interest. Bull Minèr 109: 555–573

Montel J-M, Vielzeuf D (1997) Partial melting of metagreywackes. II. Compositions of minerals and melts. Contrib Mineral Petrol 128: 176–196

Newton RC, Haselton HT (1981) Thermodynamics of the garnet-plagioclase-Al_2SiO_5-quartz geobarometer. Adv Phys Geochem 1: 131–148

Patiño Douce AE, Johnston AD (1991) Phase equilibria and melt productivity in the pelitic system: implications for the origin of peraluminous granitoids. Contrib Mineral Petrol 107: 202–218

Patiño Douce AE (1993) Titanium substitution in biotite; an empirical model with applications to thermometry, O_2 and H_2O barometries, and consequences for biotite stability. Chem Geol 108: 133–162

Patiño Douce AE, Johnston A, Rice JM (1993) Octahedral excess mixing properties in biotite; a working model with applications to geobarometry and geothermometry. Am Mineral 78: 113–131

Patiño Douce AE, Beard JS (1996) Effects of P, f(O_2) and Mg/Fe ratio on dehydration melting of model metagreywackes. J Petrol 37: 999–1024

Patiño Douce AE, Harris N (1998) Experimental constraints on Himalayan anatexis. J Petrol 39: 689–710

Platt JP, Soto JI, Comas MC, Leg 16 Shipboard Scientists (1996) Decompression and high-temperature-low-pressure metamorphism in the exhumed floor of an extensional basin, Alboran Sea, western Mediterranean. Geology 24: 447–450

Pownceby MI, Wall VJ, O'Neill HStC (1987) Fe-Mn partitioning between garnet and ilmenite: experimental calibrations and applications. Contrib Mineral Petrol 97: 116–126

Spear FS, Kohn MJ, Cheney JT (1999) P-T paths from anatectic pelites. Contrib Mineral Petrol 134: 17–32

Stevens G, Clemens JC, Droop GTR (1997) Melt production during granulite-facies anatexis: experimental data from "primitive" metasedimentary protoliths. Contrib Mineral Petrol 128: 352–370

Thompson AB (1982) Dehydration-melting of pelitic rocks and the generation of H_2O-undersaturated granitic liquids. Am J Sci 282: 1567–1595

Vielzeuf D (1983) The spinel and quartz associations from Tallante (S.E. Spain) and their potential use in geothermometry and barometry. Contrib Mineral Petrol 82: 301–311

Vielzeuf D, Holloway JR (1988) Experimental determination of the fluid-absent melting relations in the pelitic system. Consequences for crustal differentiation. Contrib Mineral Petrol 98: 257–276

Vielzeuf D, Montel JM (1994) Partial melting of metagreywackes. I. Fluid-absent experiments and phase relationships. Contrib Mineral Petrol 117: 375–393

Zeck HP (1968) Anatectic origin and further petrogenesis of almandine-bearing biotite-cordierite-labradorite-dacite with many inclusions of restite and basaltoid material, Cerro de Hoyazo, SE Spain. PhD Thesis, Amsterdam University, Amsterdam

Zeck HP (1970) An erupted migmatite from Cerro de Hoyazo, SE Spain. Contrib Mineral Petrol 26: 225–246

Zeck HP (1996) Betic-Rif orogeny: subduction of Mesozoic Tethys lithosphere under eastward drifting Iberia, slab detachment shortly before 22 Ma, and subsequent uplift and extensional tectonics. Tectonophysics 254: 1–16